Modeling Ion Transport in Tethered Bilayer Lipid Membranes. 1. Passive Ion Permeation

Joseph W. F. Robertson,[†,‡] Marcel G. Friedrich,[†,§] Asmorom Kibrom,[†] Wolfgang Knoll,[†] Renate L. C. Naumann,*[,†] and Dieter Walz[||]

Max Planck Institute for Polymer Research, Ackermannweg 10, 55128 Mainz, Germany, and Biozentrum, University of Basel, Basel, Switzerland

Received: January 8, 2008; Revised Manuscript Received: June 10, 2008

Ion transport across tethered bilayer lipid membranes (tBLMs) is modeled using a hybrid network description which combines potential-dependent rate equations with passive electrical elements. Passive permeation of ions is described by the integrated Nernst−Planck equation. Simulations based on this model are performed with the network simulation program SPICE (simulation program with integrated circuit emphasis). Electrochemical impedance spectra of tBLMs are simulated with this algorithm and challenged by spectra measured with tBLMs submersed in 0.1 M KCl solution and subjected to various potential differences. It is found that the simulated spectra can only satisfactorily represent the experimental data if the permeability coefficients of the ions are dependent on the membrane potential. It is concluded that the mechanism of passive ion transport across the tBLM seems to follow the transient pore model rather than the solubility−diffusion model. This algorithm can be easily extended to include ion transport processes due to channels, carriers, or pumps incorporated into the tBLM.

1. Introduction

Bilayer lipid membranes tethered to a metal electrode are well established as a model system for biological membranes. They have been developed with the prospect to investigate the functionality and kinetics of membrane proteins.[1−3] These proteins require an aqueous phase on either side of the lipid bilayer. For this purpose, oligo(ethylene oxide)[4] or other hydrophilic spacers had been introduced between the lipid headgroup and the metal electrode. They provide an aqueous-like compartment for ions mimicking the cytosol. A wide range of channel forming peptides and proteins has been incorporated,[5−8] suggesting that tethered bilayer lipid membranes (tBLM) can be used as a platform not only for fundamental charge transfer studies but also for chemical sensors.

Typically, electrochemical impedance spectroscopy (EIS) is used to probe the charge-transport processes across biomimetic membranes including tBLMs. Quantitative information can be extracted from impedance spectra by complex nonlinear least-squares fitting of the parameters of simple passive circuit elements (primarily capacitors and resistors) in equivalent circuits.[9] However, passive elements as, for example, ohmic resistors are not designed to represent the kinetics of ion transport. For example, an ohmic resistor has been shown to be inadequate to model the kinetics of the K^+ carrier valinomycin.[10] Attempts have been made to interpret the fitted parameter values of impedance spectra in terms of potential-dependent rate equations.[11−13] These model calculations, however, were not able to account for the electric field[11] and the concentration gradients[14] throughout the system. Hence we have designed a model that includes a mathematical description of processes across membranes besides passive electrical elements. Parameters such as concentrations and volumes can then be taken directly into account, together with the electrical potential and other electrical parameters. We will use SPICE (simulation program with integrated circuit emphasis)[15] to explore the behavior of this model[16] and to simulate electrochemical impedance spectra.

Previous and current investigations of ion transport through ion carriers,[10,17] channels,[6] and ion pumping proteins[18−20] immobilized in tBLMs provide evidence that passive ion transport not mediated by any protein needs to be modeled in the first place. Passive ion transport is the underlying process of all mediated ion transfer processes and has to be taken into account in any future model. In this context, it should be noted that we do not focus on a particular mechanism for passive ion transport. Our aim is to be able to satisfactorily model this process under the conditions pertinent to our electrochemical measurements. This applies to impedance spectra as well as to transient changes of concentrations and the potential profile across tBLMs.

2. Experimental Methods

2.1. Materials. Diphytanoylphosphatidyl choline (DphyPC) was supplied from Avanti Polar Lipids, Inc., Alabaster, AL, and potassium chloride was obtained from Sigma-Aldrich. Purified water (>18 MΩ cm) from a Milli-Q (Millipore, Inc.) system was used throughout. The synthesis of the thiolipid 2,3-di-*O*-phytanyl-*sn*-glycerol-1-tetraethylene glycol-DL-α-lipoic acid ester lipid (DPTL) was carried out as described previously.[17]

2.2. Preparation of the tBLM on Template Stripped Gold (TSG) Electrode. TSG surfaces were prepared as described previously.[21] Briefly, 50 nm thick gold films were deposited by electrothermal evaporation (rate 0.01 − 0.05 nm/s, 2×10^{-6} mbar) on silicon wafers. The gold films were then glued with epoxy EPO-TEK 353ND-4 to glass slides and cured for 60 min at 150 °C. Immediately prior to use the Au/epoxy/glass was

* Corresponding author. Tel: +49 6131 379157. Fax: +49 6131 379100. E-mail: naumannr@mpip-mainz.mpg.de.
† Max Planck Institute for Polymer Research.
‡ Present address: Electronics and Electrical Engineering Laboratory, Semiconductor Electronics Division, NIST, Gaithersburg, MD 20899-8120.
§ Present address: Department of Chemistry and Chemical Biology, Harvard University, 12 Oxford Street, Cambridge, MA 02138.
|| Biozentrum. Present address: Lerchenstrasse 21, 4059 Basel, Switzerland.

10.1021/jp800162d CCC: $40.75
Published on Web 08/05/2008

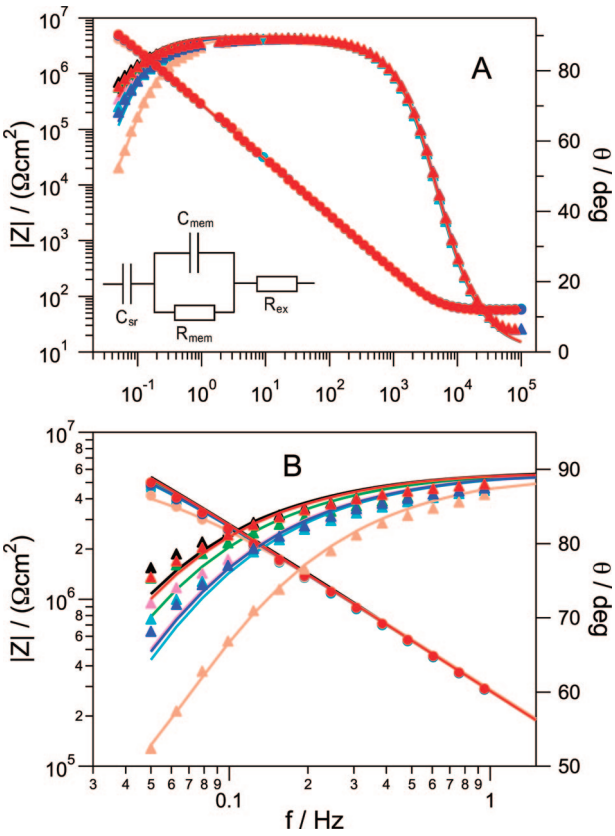

Figure 1. EIS of a tBLM at different bias potentials. (A) The magnitude of the impedance Z (circles) and the phase angle θ (triangles) are plotted as a function of frequency (Bode plot). DiPhyPC/DPTL bilayer in 0.1 M KCl solution, bias potentials of +300 mV (cyan), +200 mV (magenta), +100 mV (green), 0 mV (black), −100 mV (red), −200 mV (blue), and −300 mV (orange). The lines represent the results of fitting the parameter values of an equivalent circuit (inset and Table 1) to the spectra. (B) Blow up of Bode plot at low frequencies.

separated from the silicon wafer and immersed into a 0.2 mg/mL ethanolic DPTL solution for 24 h. After self-assembly, the surfaces were rinsed with copious amounts of ethanol, dried in a stream of nitrogen, and immediately used for vesicle fusion.

Vesicles were prepared from extrusion of a solution of 1.5 mg/mL DphyPC in pure water through a 50 nm polycarbonate filter (Avestin Inc.). The clear, colorless eluent was diluted to 0.015 mg/mL with 0.1 M KCl and immediately injected into a flow cell containing the DPTL-coated gold electrode. The tBLM formed during an overnight incubation was rinsed with 0.1 M KCl to remove the excess vesicles.

2.3. Electrochemical Measurements. EIS experiments were performed with tBLMs in 0.1 M KCl, using an EG&G 273 potentiostat/galvanostat equipped with a Solartron 1260 frequency response analyzer. Potential control and data collection were obtained with the Zplot/Zview software package (Scribner Associates, Inc.). The gold electrode, a Ag|AgCl, 3 M KCl, and a Pt wire were used in a three-electrode setup as working electrode, reference electrode, and counter electrode, respectively. The parameter values of an equivalent circuit were fitted to the spectra as described previously.[17]

3. Results

3.1. EIS of a tBLM. Figure 1 shows EIS traces for a tBLM at several different bias potentials between +0.3 V and −0.3 V vs Ag|AgCl, 3 M KCl. In the frequency range above 10 Hz, the spectra are essentially independent of the potential; however, at low frequencies they vary systematically. With increasing negative potentials, O_2 reduction begins to contribute to the low-frequency portion of the spectra. Hence the potential range was limited to −0.3 V, but it cannot be definitely excluded that O_2 reduction may contribute already at this potential.

TABLE 1: Parameter Values of Elements in the Equivalent Circuit (Inset of Figure 1A)

bias potential/V	R_{ex}/(Ω cm²)	R_{mem}/(MΩ cm²)	C_{mem}/(μF cm^{-2})	C_{sr}/(μF cm^{-2})
0.3	57.7 (0.4)[a]	8.8 (0.4)		4.7 (0.2)
0.2	57.2 (0.5)	9.4 (0.4)		4.6(0.2)
0.1	56.9 (0.5)	11.8 (0.6)		4.6 (0.2)
0[c]	56.5 (0.4)	14.2 (0.7)	0.65[b] (0.01)	4.3 (0.1)
−0.1	56.1 (0.3)	13.3 (0.6)		4.3 (0.2)
−0.2	55.8 (0.3)	8.9 (0.3)		4.2(0.1)
−0.3	55.5 (0.3)	4.8 (0.2)		3.9 (0.5)

[a] Error provided by the fitting program ZVIEW. [b] The same value of C_{mem} was used for all bias potentials to aid convergence when fitting the experimental data. [c] Literature values for R_{mem}/(MΩ cm²) and C_{mem}/(μF cm^{-2}) at zero bias potential are respectively 14.9 and 0.67,[10] 4.35 and 0.49,[17] and 18−71 and 0.64−0.72.[21]

To extract further information from these data, they were analyzed with an equivalent circuit[10,17] consisting of the resistance R_{ex} of the bulk solution, in series with the membrane, which is modeled by a parallel resistance R_{mem} and capacitance C_{mem}, and a capacitance C_{sr} representing the spacer region (Figure 1A inset). R_{ex} and C_{sr} appear to be nearly constant over the entire potential window (see Table 1). R_{mem} shows a high resistance of the membrane on the order of MΩ cm². It is potential dependent with a peak at about 0 V and decreasing both at positive and negative bias potentials. It should be mentioned that the position of the maximum is sensitive to the individual sample preparation and can vary by as much as 200 mV. The values of R_{mem} at zero bias potential and C_{mem} are in line with those for DiPhyPC/DPTL tBLMs found before (Table 1).[10,17,21]

3.2. Development of the Model. Models that describe passive ion permeation through phospholipid bilayers have been developed on the basis of the solubility−diffusion theory which, however, proved unsatisfactory particularly for small ions such as Na^+.[22] Alternative models were introduced in terms of hydrated transient defects produced by thermal fluctuations of the lipid molecules. This model seems to apply for halide ions when the lipid layer is thin enough.[22,23] However, a model of general applicability has so far not been agreed upon. Moreover, as mentioned in the Introduction, for the time being we do not focus on particular mechanisms but adopt a basic approach by using the integrated Nernst−Planck equation.[24] It relates the flux j_i of the ith ion (i.e., the flow per unit membrane area) to the permeability coefficient P_i, the ion concentrations $c_{i,1}$ and $c_{i,2}$ on either side of the membrane, and the membrane potential $\Delta\varphi_m$, defined as the difference in electrical potential across the membrane

$$j_i = P_i \frac{z_i F \Delta\varphi_m}{RT} \frac{c_{i,1} \exp\{z_i F \Delta\varphi_m/(RT)\} - c_{i,2}}{\exp\{z_i F \Delta\varphi_m/(RT)\} - 1}; \quad \Delta\varphi_m = \varphi_1 - \varphi_2 \quad (1)$$

Here z_i is the charge number of the ion, while R, T, and F have their usual meaning. The electrical current density associated with the ion flux is then given by

$$i_i = z_i F j_i \quad (2)$$

Strictly speaking, activities should be used in eq 1, however, for thepresent purpose it is legitimate to approximate them by concentrations.

The concentration of the ith ion in the bulk solution, $c_{i,\mathrm{ex}}$ ($c_{i,2}$ in eq 1) can be assumed to be constant. The concentration in the submembrane space, $c_{i,\mathrm{in}}$ ($c_{i,1}$ in eq 1) changes with time due to the flow j_i

$$\mathrm{d}c_{i,\mathrm{in}}/\mathrm{d}t = j_i/V_{\mathrm{in}} \quad (3)$$

where V_{in} is the volume of the submembrane space per unit area. The electrical potential profile across the tBLM can be split into different components

$$\varphi_{\mathrm{el}} - \varphi_{\mathrm{bs}} = \Delta\phi_{\mathrm{msp}} + \Delta\varphi_{\mathrm{sr}} + \Delta\varphi_{\mathrm{m}} + \Delta\varphi_{\mathrm{ex}} \quad (4)$$

Here φ_{el} and φ_{bs} are the Galvani potentials within the gold electrode and the bulk of the electrolyte solution, respectively. These potentials are with respect to the (metal terminal of the) Ag|AgCl, 3 M KCl reference electrode. In eq 4, $\Delta\varphi_{\mathrm{msp}}$ denotes the metal surface dipole potential. Since the spacer region is not an aqueous phase (J. Lipkowski, personal communication) a diffuse layer adjacent to the gold surface cannot be expected. Instead, we introduce the capacitance C_{sr}, which accounts for the balance of charges at the gold surface, and $\Delta\varphi_{\mathrm{sr}}$ then denotes the potential difference across C_{sr}. Moreover, $\Delta\varphi_{\mathrm{ex}}$ denotes the potential drop in the electrolyte solution due to the electrical current density i_{el} running through the system

$$\Delta\varphi_{\mathrm{ex}} = R_{\mathrm{ex}} i_{\mathrm{el}} \quad (5)$$

In eq 4, the rather small potential difference across the diffuse layer at the membrane/bulk solution interface is neglected.[25] Inserting eq 5 into eq 4 and rearranging yields

$$i_{\mathrm{el}} = (\varphi_{\mathrm{el}} - \Delta\varphi_{\mathrm{sr}} - \Delta\varphi_{\mathrm{m}} - \Delta\varphi_{\mathrm{sp,bs}})/R_{\mathrm{ex}} \quad (6)$$

with the abbreviation

$$\Delta\varphi_{\mathrm{sp,bs}} = \Delta\varphi_{\mathrm{msp}} + \varphi_{\mathrm{bs}} \quad (7)$$

The time dependence of $\Delta\varphi_{\mathrm{m}}$ is given by

$$\mathrm{d}\Delta\varphi_m/\mathrm{d}t = \left(i_{\mathrm{el}} - \sum\nolimits_i i_i\right)/C_{\mathrm{mem}} \quad (8)$$

where $\sum_i i_i$ means the sum over the current densities associated with the permeation of all ions (cf. eq 2). The time dependence of $\Delta\varphi_{\mathrm{sr}}$ is given by

$$\mathrm{d}\Delta\varphi_{\mathrm{sr}}/dt = i_{\mathrm{el}}/C_{\mathrm{sr}} \quad (9)$$

3.3. Simulation Procedure. Numerical integration of eqs 3, 8, and 9 together with eqs 1, 2, and 6 yields the time course of the current density i_{el}, the ion concentrations $c_{i,\mathrm{in}}$ in the submembrane space, and the potential differences $\Delta\varphi_{\mathrm{m}}$ and $\Delta\varphi_{\mathrm{sr}}$, starting from given initial conditions. The constant bias potential is assigned to φ_{el}, to which a small signal ac voltage is added when needed.

A convenient alternative to numerically integrating the differential equations is to express the model in a network representation and to use the software package SPICE for simulating its behavior.[16] The advantage of this method is the modular design of the model which also reflects its topology and allows rapid alterations and extensions of the model. No differential equations have to be formulated because they are automatically generated by SPICE when analyzing the circuit. A description of this procedure for the present model can be found in the Supporting Information.

3.4. Assignment of Parameter Values. For the electrical elements, average values of the fitted parameters given in Table 1 are used, i.e., $C_{\mathrm{mem}} = 0.65\ \mu\mathrm{F\ cm^{-2}}$, $C_{\mathrm{sr}} = 4.3\ \mu\mathrm{F\ cm^{-2}}$, and $R_{\mathrm{ex}} = 56\ \Omega\ \mathrm{cm^2}$. As a first approximation, we assume $\Delta\varphi_{\mathrm{sp,bs}} \approx 0$, i.e., the metal surface dipole potential and the bulk phase potential balance out each other (cf. eq 7). Parameters pertaining to ion permeation are $c_{\mathrm{K,ex}} = c_{\mathrm{Cl,ex}} = 0.1$ M, and $V_{\mathrm{in}} = 0.22\ \mathrm{nL\ cm^{-2}}$, which can be estimated from the length of the spacer.[10] Moreover, $z_{\mathrm{K}} = 1$, $z_{\mathrm{Cl}} = -1$, and the temperature is 25 °C. The assignment of values to the permeability coefficients P_{K} and P_{Cl} for K^+ and Cl^- requires more detail. According to eq 1, the flux of the ith ion at equal concentrations on both sides of the membrane, $c_{i,1} = c_{i,2} = c_i$, is

$$j_i = P_i z_i c_i F \Delta\varphi_m/(RT) \quad (10)$$

Hence the current density due to permeation of K^+ and Cl^- across the membrane at $c_{\mathrm{K}} = c_{\mathrm{Cl}} = c_{\mathrm{KCl}}$ amounts to (cf. eq 2)

$$i = F(z_{\mathrm{K}} j_{\mathrm{K}} + z_{\mathrm{Cl}} j_{\mathrm{CL}}) = \Delta\varphi_{\mathrm{m}}\left[F^2 c_{\mathrm{KCl}}\left({z_{\mathrm{K}}}^2 P_{\mathrm{K}} + {z_{\mathrm{Cl}}}^2 P_{\mathrm{Cl}}\right)/(RT)\right] = \Delta\varphi_{\mathrm{m}}/R_{\mathrm{mem}} \quad (11)$$

and can be related to the resistance of the membrane R_{mem} determined under the particular conditions, as shown in eq 11. A total permeability coefficient can then be defined as

$$P_{\mathrm{tot}} = {z_{\mathrm{K}}}^2 P_{\mathrm{K}} + {z_{\mathrm{Cl}}}^2 P_{\mathrm{Cl}} = RT/\left(F^2 c_{\mathrm{KCl}} R_{\mathrm{mem}}\right) \quad (12)$$

and related to R_{mem}. With the ratio of coefficients $p = P_{\mathrm{K}}/P_{\mathrm{Cl}}$ we obtain

$$P_{\mathrm{K}} = P_{\mathrm{tot}} p/\left({z_{\mathrm{K}}}^2 p + {z_{\mathrm{Cl}}}^2\right) \quad \text{and} \quad P_{\mathrm{Cl}} = P_{\mathrm{tot}}/\left({z_{\mathrm{K}}}^2 p + {z_{\mathrm{Cl}}}^2\right) \quad (13)$$

$R_{\mathrm{mem}} = 14.2\ \mathrm{M\Omega\ cm^2}$ at zero bias potential of the tBLM (Table 1) yields $P_{\mathrm{tot}} = 1.9 \times 10^{-10}$ cm/s (eq 12). P_{K} seems to be larger than P_{Cl} because of the stronger effect of negative bias potentials on impedance and phase angle at low frequencies than that of positive bias potentials (see Figure 1), hence $p = 10$ was chosen.

3.5. Simulated Impedance Spectra. Spectra were simulated in three steps essentially following the experimental protocol. First the tBLM was formed at zero bias potential and 0.1 M KCl in the bulk solution. In this step, the ions partition into the submembrane space, which is simulated with $\varphi_{\mathrm{el}} = 0$ and the initial conditions $c_{\mathrm{K,in}} = c_{\mathrm{Cl,in}} = \Delta\varphi_{\mathrm{m}} = \Delta\varphi_{\mathrm{sr}} = 0$. Because $P_{\mathrm{K}} > P_{\mathrm{Cl}}$, initially the flux of K^+ is larger than that of Cl^-, causing $c_{\mathrm{K,in}}$ to rise faster than $c_{\mathrm{Cl,in}}$ (Figure 2A). This asymmetry induces a current across the membrane which charges the membrane capacitance thus generating a membrane potential $\Delta\varphi_{\mathrm{m}}$ (Figure 2B). Concomitantly the potential difference $\Delta\varphi_{\mathrm{sr}} = -\Delta\varphi_{\mathrm{m}}$ is formed because φ_{el} is clamped to zero. With increasing time $\Delta\varphi_{\mathrm{m}}$ and $\Delta\varphi_{\mathrm{sr}}$ gradually collapse while $c_{\mathrm{K,in}}$ and $c_{\mathrm{Cl,in}}$ essentially coincide, and the equilibrium state is eventually attained where $c_{\mathrm{K,in}} = c_{\mathrm{Cl,in}} = 0.1$ M and $\Delta\varphi_{\mathrm{m}} = \Delta\varphi_{\mathrm{sr}} = 0$. Note that after about 12 h $c_{\mathrm{K,in}}$, $c_{\mathrm{Cl,in}}$, $\Delta\varphi_{\mathrm{m}}$, and $\Delta\varphi_{\mathrm{sr}}$ have essentially reached their equilibrium values.

In the second step, different bias potentials were applied. The ions then repartition and a new equilibrium state is attained. This is simulated with φ_{el} set to the respective bias potential, and the initial conditions $c_{\mathrm{K,in}} = c_{\mathrm{Cl,in}} = 0.1$ M, $\Delta\varphi_{\mathrm{m}} = \Delta\varphi_{\mathrm{sr}} = 0$. In a fast process with a relaxation time $\tau = R_{\mathrm{ex}}\left({C_{\mathrm{mem}}}^{-1} + {C_{\mathrm{sr}}}^{-1}\right)^{-1} \approx 32\ \mu\mathrm{S}$ (not shown in Figure 3) C_{mem} and C_{sr} are charged, and the respective potential differences built up are as expected for two capacitors in series, i.e.

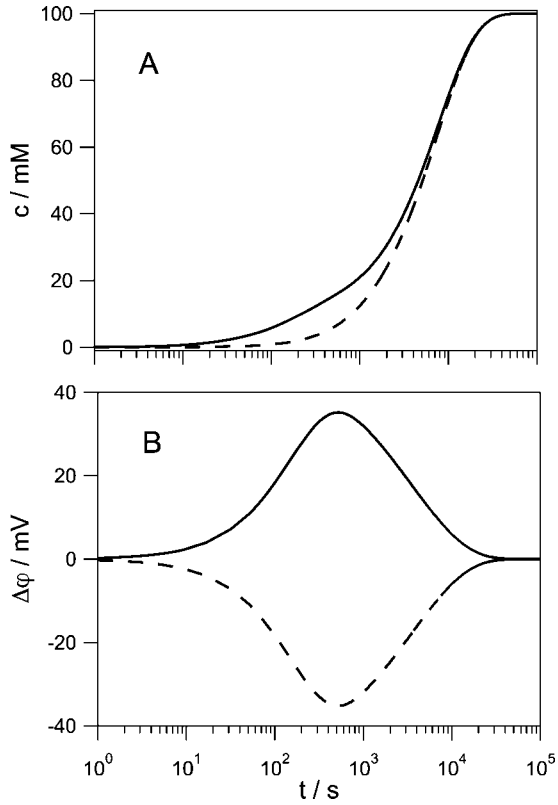

Figure 2. Simulation of ion equilibration during formation of the tBLM in 0.1 M KCl solution: (A) ion concentrations $c_{K,in}$ (solid line) and $c_{Cl,in}$ (broken line) in the submembrane space, (B) potential differences $\Delta\varphi_m$ (solid line) and $\Delta\varphi_{sr}$ (broken line). Note the logarithmic time scale.

$$\Delta\varphi_m = \varphi_{el}C_{sr}/C_{mem} + C_{sr} \quad \text{and} \quad \Delta\varphi_{sr} = \varphi_{el}C_{mem}/(C_{mem} + C_{sr}) \quad (14)$$

The altered membrane potential initiates the considerably slower ion permeation, which discharges the membrane capacitance thus causing $|\Delta\varphi_m|$ to decrease. Concomitantly, $|\Delta\varphi_{sr}|$ increases since φ_{el} is clamped, so that at equilibrium 97% of the applied potential drops across the capacitance C_{sr} (Figure 3, A and B). The time course of the ion concentrations in the submembrane space is biphasic. As expected, the final values of $c_{K,in}$ are larger and smaller while those for $c_{Cl,in}$ are smaller and larger than those at zero bias potential for positive and negative bias potentials, respectively (Figure 3, C and D). Again, it takes about 12 h for the variables $c_{K,in}$, $c_{Cl,in}$, $\Delta\varphi_m$, and $\Delta\varphi_{sr}$ to reach values close to those at equilibrium.

As a control, the simulations in both steps were repeated with different values for P_{tot} and p. This altered the time courses of the variables, but the constant values eventually reached for all variables were always those shown in Figures 2 and 3, as it should be for true equilibrium states. Moreover, simulations in step 2 were performed with different values for C_{mem} and C_{sr}. Varying C_{mem} at a constant $C_{sr} = 4.3$ μF cm^{-2} has very little effect on the time courses of $c_{K,in}$ and $c_{Cl,in}$, yielding essentially the same result as shown in Figure 3, C and D. The potential differences formed in the fast initial phase differ (cf. eq 14) but the constant values eventually reached are practically equal to those shown in Figure 3, A and B. On the other hand, varying C_{sr} at a constant $C_{mem} = 0.65$ μF cm^{-2} yields similar time courses for $c_{K,in}$ and $c_{Cl,in}$ but with equilibrium values which vary considerably depending on the particular value of C_{sr}. However, the potential differences, starting from the values according to eq 14, reach values at equilibrium which are close to those shown in Figure 3A,B, indicating a potential drop across the capacitance C_{sr} between 99% and 90% of the applied potential for C_{sr} between 2 and 20 μF cm^{-2}, respectively.

In the third step, EIS was performed. Here, each frequency has to be simulated separately, using the equilibrium values for $c_{K,in}$, $c_{Cl,in}$, $\Delta\varphi_m$, and $\Delta\varphi_{sr}$ from the simulations in the second step as initial conditions. A sinusoidal ac voltage with amplitude 10 mV and the given frequency is added to the respective bias potential assigned to φ_{el}. The ac voltage elicits oscillations of $c_{K,in}$, $c_{Cl,in}$, $\Delta\varphi_m$, and $\Delta\varphi_{sr}$ whose baselines, except for that of $\Delta\varphi_m$, initially change with time (Figure 4A−D). When constant baselines are reached, the current density i_{el} and the electrode potential φ_{el} (Figure 4, E and F) are used to calculate the impedance Z and the phase angle θ by means of a nonlinear fitting program (IGOR), and the spectra thus obtained for different bias potentials are shown in Figure 5. In the case of zero bias potential, both Z and θ agree well with the experimental data (Figure 1), except for a deviation in θ at frequencies larger than 20 kHz, which is most likely due to stray capacitances in the measuring system. However, only a slight dependence of θ on the applied bias potential at low frequencies is detectable and even in the wrong direction for positive potentials, while hardly any change in Z occurs, both in contrast to the experimental data. Choosing p values larger than 10 has little effect, while decreasing p diminishes the existing slight dependence of θ on the bias potential. It is thus evident that the experimentally observed decrease in membrane resistance for positive and negative bias potentials and the corresponding differences in phase angle at low frequencies cannot be explained by the different ion concentrations in the submembrane space and different permeability coefficients for K^+ and Cl^-. Therefore, the description of ion transport through the membrane has to be refined.

In a simple mechanistic model, permeation is described by a single jump of the ith ion across the hydrophobic barrier of the membrane, and a partitioning of the ion between the aqueous phase and the layer of polar head groups. If ion partitioning is assumed to be much faster than the transfer across the hydrophobic barrier, it is always very close to equilibrium and can be assessed by the partitioning coefficient γ_i. This coefficient is determined by the difference in free energy of the ion in the headgroup layer and the aqueous phase, and the dipole potential at the membrane surface. According to the absolute rate theory[26] the rate constant of the single jump consists of an intrinsic rate constant and a Boltzmann factor $\exp[-\Delta G_i^{\ddagger}/(RT)]$. $\Delta G_i^{\ddagger}$ is the difference in free energy of the ion at the transition state and in the headgroup layer,

$$\Delta G_i^{\#} = \Delta H_i^{\#} + z_iF(\Delta\varphi_o^{\ddagger} \pm \Delta\varphi_m/2) = \Delta G_{i,o}^{\ddagger} \pm z_iF\Delta\varphi_m/2 \quad (15)$$

where the plus or minus sign for $\Delta\varphi_m$ pertains to the jump from side 2 to 1 or side 1 to 2, respectively. $\Delta H_i^{\ddagger}$ denotes the enthalpy difference and $\Delta\varphi_o^{\ddagger}$ is the contribution from the constant electrical potential profile across the hydrophobic barrier. Here it is assumed that the transition state is located at the center of the hydrophobic phase. If intrinsic rate constant multiplied by the Boltzmann factor $\exp[-\Delta G_{i,o}^{\ddagger}/(RT)]$ is abbreviated by $k_{i,o}$ the ion flux becomes

$$j_i = k_{i,o}\gamma_i\{c_{i,1}\exp[z_iF\Delta\varphi_m/(2RT)] - c_{i,2}\exp[-z_iF\Delta\varphi_m/(2RT)]\} \quad (16)$$

Simulations were performed as described above with eq 16

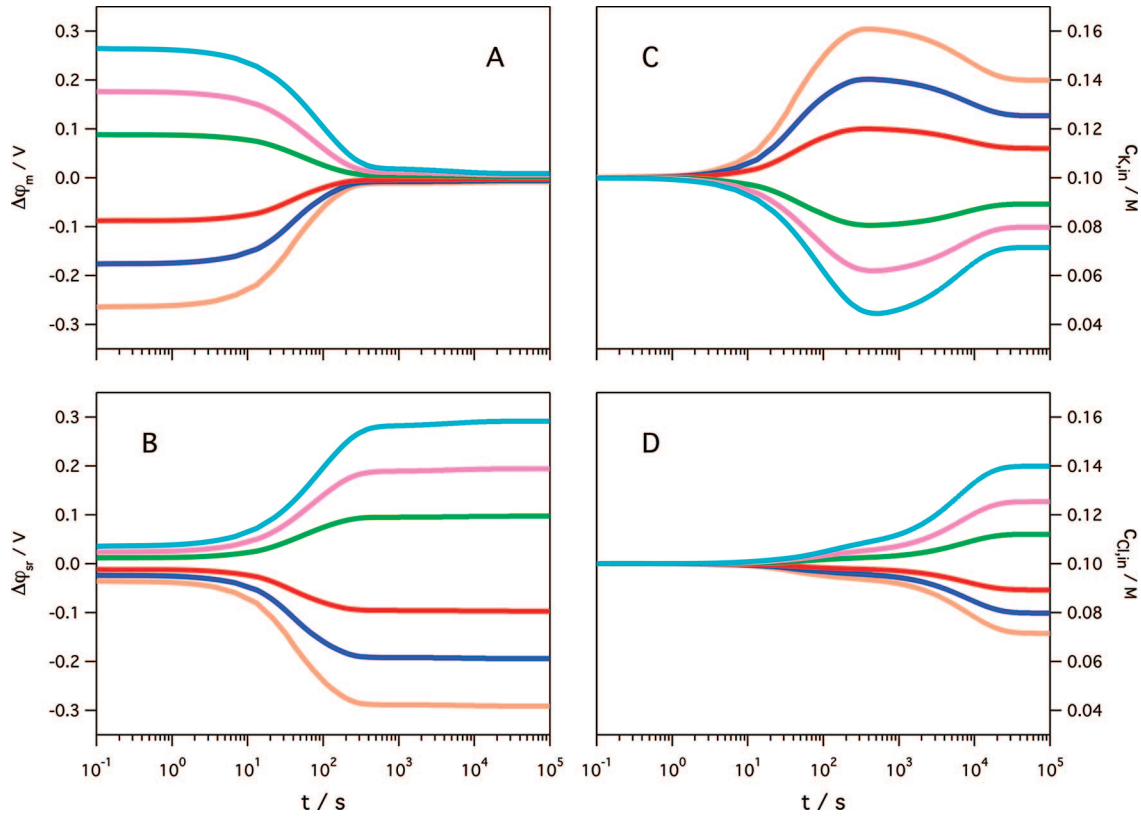

Figure 3. Simulation of the re-equilibration of ions when different bias potentials are applied to the pre-equilibrated tBLM: potential differences $\Delta\varphi_m$ (A) and $\Delta\varphi_{sr}$ (B), ion concentrations $c_{K,in}$ (C), and $c_{Cl,in}$ (D) in the submembrane space. Color code for bias potentials as in Figure 1, i.e., +300 mV (cyan), +200 mV (magenta), +100 mV (green), −100 mV (red), −200 mV (blue), and −300 mV (orange). Note the logarithmic time scale.

replacing eq 1. Since the term $k_{i,o}\gamma_i$ is equivalent to the permeability coefficient P_i the same values can be used. The results are not shown because they are identical with those in Figures 2−5. Using $p = 0.000\,29$, as should be expected for a solubility−diffusion type of model (see Discussion) yields the same Bode plots as in Figure 5, however, with the slight dependence on the bias potential being inversed, i.e., curves for positive bias potentials coincide with those for the respective negative bias potentials for $p = 10$, and vice versa. Thus, it appears that the model is rather insensitive to the type of transport chosen. Moreover, it is evident that any further refinements, such as more than one step across the hydrophobic barrier or different surface potentials at both sides of the membrane for the mechanistic model, or a space-dependent mobility of the ion for the integrated Nernst−Planck equation, would be useless because the pertinent parameters are not affected by different membrane potentials. Hence, no further attempts were made to refine the model in this respect.

A generalized form of the Nernst−Planck equation includes image forces for the partitioning of ions into the membrane. When integrated, it yields a nonlinear dependence of the ion transport on the membrane potential $\Delta\varphi_m$.[27] However, an appreciable deviation from linearity occurs only for $|\Delta\varphi_m| >$ ~25 mV, which is larger than the $\Delta\varphi_m$ values found in the simulations (cf. Figures 3A and 4C). A nonlinear dependence arises also if ion transport occurs through pores, which result from thermal fluctuations of the lipid molecules. Potential pulse experiments with UO_2^{2+}-modified BLMs have shown that the formation rate constant of pores $k_{p,f}$ is dependent on $\Delta\varphi_m$, i.e., $k_{p,f} \propto \exp[(\Delta\varphi_m/K_s)^2]$, where K_s is a scaling factor.[28,29] The resealing of the pores is a first-order process with a rate constant $k_{p,r}$ which appears to be independent of $\Delta\varphi_m$, and hence the number of pores at steady state is proportional to $\exp[(\Delta\varphi_m/K_s)^2]$. Since the total permeability of the membrane is proportional to the number of pores

$$P_{tot}(\Delta\varphi_m) = P_{tot}(0)\exp\left[(\Delta\varphi_m/K_s)^2\right] \qquad (17)$$

where $P_{tot}(0)$ denotes the total permeability coefficient at $\Delta\varphi_m = 0$ arising from the intrinsic steady state number of pores. The scaling factor is related to the thickness of the membrane d_m and its dielectric constant ε_m, as well as to the dielectric constant of the aqueous phase ε_w

$$K_s = \left\{2d_m kT/\left[\pi r_h^{*2}\varepsilon_o(\varepsilon_w - \varepsilon_m)\right]\right\}^{1/2} \qquad (18)$$

where k is Boltzmann's constant and ε_o the absolute permittivity, while r_h^* denotes a critical radius for pore formation.

Simulations of impedance spectra were performed with P_{tot} in eq 13 substituted from eq 17, and with $P_{tot}(0) = 1.9 \times 10^{-10}$ cm/s and $p = 10$ as before. Since the actual values of $k_{p,f}$ and $k_{p,r}$ are not known, and eq 17 pertains to the steady state of pore formation only, a constant value for $\Delta\varphi_m$ is used as an approximation and set equal to the value reached at equilibrium in step 2. Moreover, the value of r_h^* for tBLMs cannot be obtained independently, hence K_s had to be adjusted and was found to be 8.3 mV. The simulated spectra (Figure 6) now represent the experimental data reasonably well, thus corroborating the concept of a nonlinear dependence of ion transport on the membrane potential in tBLMs.

4. Discussion

The simulation of impedance spectra employing a model for ion permeation instead of a passive membrane resistance has several advantages. It provides insight into the mechanism and

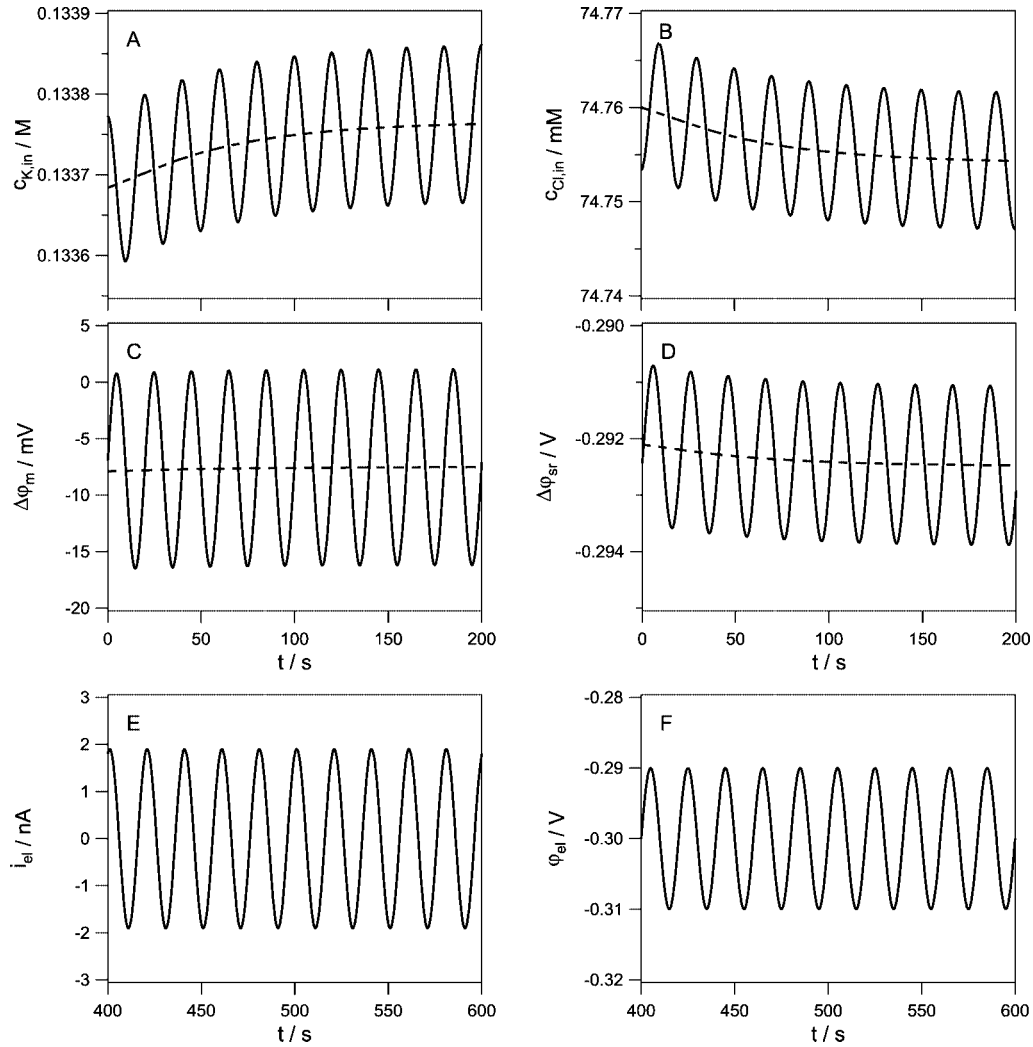

Figure 4. Example for the simulated response of ion concentrations $c_{K,in}$ (A) and $c_{Cl,in}$ (B), and potential differences $\Delta\varphi_m$ (C) and $\Delta\varphi_{sr}$ (D) to a sinusoidal ac voltage. Initially, the baselines of the oscillations vary (broken lines). When constant baselines are reached, the current density i_{el} (E) and the electrode potential φ_{el} (F) are analyzed for impedance and phase angle. Bias potential −300mV, ac amplitude 10 mV, and frequency 50 mHz.

can cope with specificities of the different ion species involved. Moreover, it provides access to different parameters that are experimentally inaccessible, and thus can help to understand the behavior of the system under the influence of various conditions. It can be deduced, for example, that the equilibration process of monovalent ions due to passive permeation can take quite a long time of up to several hours if reasonable permeability coefficients are used. Another significant result is the distribution of potential differences across the layered structure following the application of different bias potentials. Only in a short initial phase, before any appreciable ion transport does occur, the applied potential drops mainly across the lipid membrane, as intuitively expected from the 5-fold lower capacitance of the membrane compared to that associated with the spacer region, and the high resistance of the lipid bilayer. However, in the course of the repartitioning of ions, this distribution is shifted toward the spacer region and, after equilibration of the ions, almost all of the applied potential drops across the capacitance C_{sr}, which accounts for the balance of charges at the gold surface.

The parameter directly accessible from the impedance spectra is the total coefficient P_{tot} for permeation of K^+ and Cl^- across the bilayer of the tBLM. Its value (1.9×10^{-10} cm/s) compares well with that (0.8×10^{-10} cm/s) which can be calculated with representative values for the permeability coefficients of both ions for freely suspended BLMs ($P_K = 5 \times 10^{-12}$ cm/s, $P_{Cl} = 7.5 \times 10^{-11}$ cm/s).[30] On the other hand, Paula et al.[22,23] have reported values of permeability coefficients for phosphatidylcholine liposomes with different thickness d_h for the hydrophobic region of the membrane. With $C_{mem} = 0.65$ μF cm^{-2} (Table 1) and a dielectric constant of 2, one obtains $d_h = 2.7$ nm for the tBLM, and the corresponding permeability coefficients for liposomes are $P_K = 3.5 \times 10^{-12}$ cm/s and $P_{Cl} = 1.21 \times 10^{-8}$ cm/s $\approx P_{tot}$. Thus, tBLMs seem to resemble more BLMs rather than liposome membranes.

The relative contributions of P_K and P_{Cl} to P_{tot}, expressed by the ratio $p = P_K/P_{Cl}$, can be inferred from the dependence of the EIS spectra on the bias potential. Although the data do not lend themselves for a precise estimation, $p = 10$ appears to be an appropriate value. This is of similar order of magnitude but reciprocal to what was found for BLMs ($p = 0.067$). But even this high ratio does not suffice to describe the potential dependence of the impedance spectra, and a dependence of the permeability coefficients on the membrane potential had to be introduced. This is interesting from the mechanistic point of view because it is in accordance with a pore model of ion permeation,[28,29] in contrast to the solubility–diffusion model proposed for liposomes.[23] A pore model is also supported by p

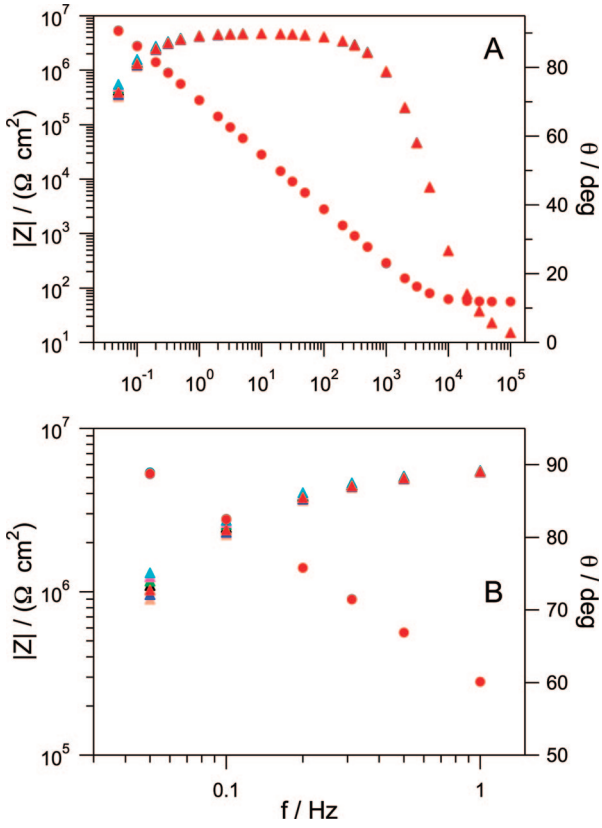

Figure 5. Impedance spectra simulated with constant permeability coefficients of ions: (A) magnitude of the impedance Z (circles) and phase angle θ (triangles) as a function of frequency (Bode plot) for bias potentials (color code as in Figure 1) +300 mV (cyan), +200 mV (magenta), +100 mV (green), 0 mV (black), −100 mV (red), −200 mV (blue), and −300 mV (orange). $P_{tot} = 1.9 \times 10^{-10}$ cm/s and $p = 10$. (B) Blow up of Bode plot at low frequencies.

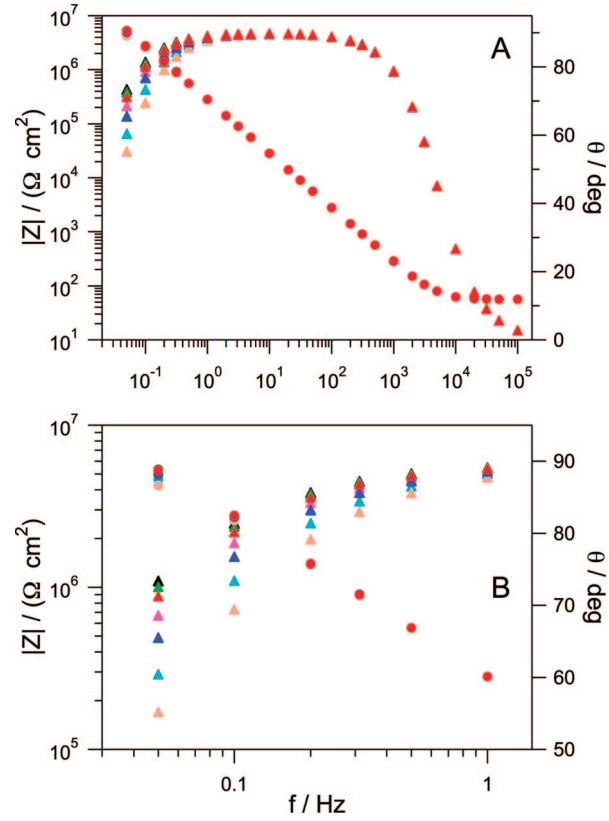

Figure 6. Impedance spectra simulated with membrane potential-dependent permeability coefficients of ions. (A) Magnitude of the impedance Z (circles) and phase angle θ (triangles) as a function of frequency (Bode plot) for bias potentials (color code as in Figure 1) +300 mV (cyan), +200 mV (magenta), +100 mV (green), 0 mV (black), −100 mV (red), −200 mV (blue), and −300 mV (orange). Dependence of P_{tot} on $\Delta\varphi_m$ according to eq 17 with $P_{tot}(0) = 1.9 \times 10^{-10}$ cm/s, $K_s = 8.3$ mV, and $p = 10$. (B) Blow up of Bode plot at low frequencies.

> 1. From eqs 15 and 16, which pertain to a solubility–diffusion type of model, it follows that $p = k_{K,o}\gamma_K/k_{Cl,o}\gamma_{Cl} \propto \exp[-2F\Delta\varphi_o^{\ddagger}/(RT)] < 1$ since $\Delta\varphi_o^{\ddagger}$ is positive (typically 0.2−0.4 V),[31] as is indeed found for liposome membranes ($p = 0.000\,29$) and BLMs. On the other hand, the pores eventually resulting from thermal fluctuations of the lipids are hydrophilic and provide an aqueous path for the ions through the membrane.[29] Neither the dipole potentials at the membrane surfaces nor the electrical potential profile across the hydrophobic barrier are then relevant. The potential profile across a hydrophilic pore is much smaller than across the lipid bilayer, and the permeability coefficients are predominantly determined by the mobility of the ions in the pore, which depends on the ion radius. Hence $p > 1$ can be expected.

For the sample preparation shown in Figure 1, the metal surface dipole potential and the potential in the bulk solution seem indeed to balance out each other, as had been assumed as a first approximation when setting $\Delta\varphi_{sp,bs} \approx 0$. This is reflected in the position of the maximum of R_{mem} at zero bias potential (Table 1). However, this need not be true for other preparations, and the maximum of R_{mem} is then shifted to nonzero bias potentials. In such a case this potential shift has to be assigned to $\Delta\varphi_{sp,bs}$ in the simulations. Thus, the bias potential dependence of the impedance spectra combined with the simulations provides some information about the metal surface dipole potential, a quantity which is generally hard to access.

5. Conclusions

Passive ion permeation plays a role in many electrochemical experiments with tethered bilayer lipid membranes (tBLMs) and thus contributes to the behavior of this system. A model for ion permeation was designed which can conveniently be analyzed using the network simulation program SPICE. It is found that electrochemical impedance spectra of tBLMs and their dependence on the applied bias potential can only be satisfactorily simulated if the permeability coefficient for cations is larger than that for anions, and both coefficients are dependent on the membrane potential. This suggests that ion permeation in tBLMs occurs more likely through transient pores rather than by a solubility−diffusion mechanism. The SPICE circuit presented here accounts for passive ion permeation and thus provides a realistic baseline for simulations of more complex systems. Because of its modular design, it can be easily extended to account also for other kinds of ion transport processes due to channels, carriers or pumps incorporated into tBLMs.

Supporting Information Available: Model Simulations with SPICE. This material is available free of charge via the Internet at http://pubs.acs.org.

References and Notes

(1) Guidelli, R.; Aloisi, G.; Becucci, L.; Dolfi, A.; Moncelli, M. R.; Buoninsegni, F. T. *J. Electroanal. Chem.* **2001**, *504*, 1–28.

(2) Knoll, W.; Morigaki, K.; Naumann, R.; Sacca, B.; Schiller, S.; Sinner, E. K. *Ultrathin Electrochemical Chemo- and Biosensors, Technology and Performance*; Mirsky, V. M., Ed.; Springer: Berlin, 2004; p 239.

(3) Sinner, E. K.; Knoll, W. *Curr. Opin. Chem. Biol.* **2001**, *5*, 705–711.

(4) Cornell, B. A.; Braach-Maksvytis, V. L. B.; King, L. G.; Osman, P. D. J.; Raguse, B.; Wieczorek, L.; Pace, R. J. *Nature* **1997**, *387*, 580–583.

(5) Becucci, L.; Guidelli, R.; Peggion, C.; Toniolo, C.; Moncelli, M. R. *J. Electroanal. Chem.* **2005**, *576*, 121–128.

(6) He, L. H.; Robertson, J. W. F.; Li, J.; Karcher, I.; Schiller, S. M.; Knoll, W.; Naumann, R. *Langmuir* **2005**, *21*, 11666–11672.

(7) Glazier, S. A.; Vanderah, D. J.; Plant, A. L.; Bayley, H.; Valincius, G.; Kasianowicz, J. J. *Langmuir* **2000**, *16*, 10428–10435.

(8) Valincius, G.; McGillivray, D. J.; Febo-Ayala, W.; Vanderah, D. J.; Kasianowicz, J. J.; Losche, M. *J. Phys. Chem. B* **2006**, *110*, 10213–10216.

(9) Macdonald, J. R. *Impedance Spectroscopy: Emphasizing Solid Materials and Systems*, 2nd ed.; Barsoukov, E., Macdonald, J. R., Eds.; Wiley: Hoboken, NJ, 2005; p 188.

(10) Naumann, R.; Walz, D.; Schiller, S. M.; Knoll, W. *J. Electroanal. Chem.* **2003**, *550*, 241–252.

(11) Becucci, L.; Moncelli, M. R.; Naumann, R.; Guidelli, R. *J. Am. Chem. Soc.* **2005**, *127*, 13316–13323.

(12) Steinem, C.; Janshoff, A.; Galla, H. J.; Sieber, M. *Bioelectrochem. Bioenerg.* **1997**, *42*, 213–220.

(13) Vallejo, A. E.; Gervasi, C. A. *Bioelectrochemistry* **2002**, *57*, 1–7.

(14) Krishna, G.; Schulte, J.; Cornell, B. A.; Pace, R. J.; Osman, P. D. *Langmuir* **2003**, *19*, 2294–2305.

(15) Vladimirescu, A. *The SPICE Book*; Wiley: New York, 1994.

(16) Walz, D.; Caplan, S. R.; Scriven, D. R. L.; Mikulecky, D. C. *Bioelectrochemistry: General Introduction*; Caplan, S. R., Miller, I. R., Milazzo, G., Eds.; Bioelectrochemistry: Principles and Practice; Birkhäuser: Basel, Switzerland, 1995; Vol. 1, p 49.

(17) Schiller, S. M.; Naumann, R.; Lovejoy, K.; Kunz, H.; Knoll, W. *Angew. Chem., Int. Ed.* **2003**, *42*, 208–211.

(18) Naumann, R.; Schmidt, E. K.; Jonczyk, A.; Fendler, K.; Kadenbach, B.; Liebermann, T.; Offenhäusser, A.; Knoll, W. *Biosens. Bioelectron.* **1999**, *14*, 651–662.

(19) Naumann, R.; Baumgart, T.; Gräber, P.; Jonczyk, A.; Offenhäusser, A.; Knoll, W. *Biosens. Bioelectron.* **2002**, *17*, 25–34.

(20) Giess, F.; Friedrich, M. G.; Heberle, J.; Naumann, R. L.; Knoll, W. *Biophys. J.* **2004**, *87*, 3213–3220.

(21) Naumann, R.; Schiller, S. M.; Giess, F.; Grohe, B.; Hartman, K. B.; Karcher, I.; Köper, I.; Lübben, J.; Vasilev, K.; Knoll, W. *Langmuir* **2003**, *19*, 5435–5443.

(22) Paula, S.; Volkov, A. G.; VanHoek, A. N.; Haines, T. H.; Deamer, D. W. *Biophys. J.* **1996**, *70*, 339–348.

(23) Paula, S.; Volkov, A. G.; Deamer, D. W. *Biophys. J.* **1998**, *74*, 319–327.

(24) Walz, D.; Caplan, S. R. *Bioelectrochemistry: General Introduction*; Caplan, S. R., Miller, I. R., Milazzo, G., Eds.; *Bioelectrochemistry: Principles and Practice*; Birkhäuser: Basel, Switzerland, 1995; Vol. 1, p 1.

(25) Becucci, L.; Moncelli, M. R.; Guidelli, R. *Langmuir* **2003**, *19*, 3386–3392.

(26) Glasstone, S.; Laidler, K. J.; Eyring, H. *The Theory of Rate Processes*; McGraw-Hill: New York, 1941.

(27) Neumcke, B.; Läuger, P. *Biophys. J.* **1969**, *9*, 1160–1170.

(28) Glaser, R. W.; Leikin, S. L.; Chernomordik, L. V.; Pastushenko, V. F.; Sokirko, A. I. *Biochim. Biophys. Acta* **1988**, *940*, 275–287.

(29) Chizmadzhev, Y. A.; Teissié, J.; Walz, D. *Bioelectrochemistry of Membranes*; Walz, D., Teissié, J., Milazzo, G., Eds.; *Bioelectrochemistry: Principles and Practice*; Birkhäuser: Basel, Switzerland, Vol. 6, 2004; p 173.

(30) Stryer, L. *Biochemistry*, 2nd ed.; W. H. Freeman: New York, 1981; p 215.

(31) Freites, J. A.; Tobias, D. J.; von Heijne, G.; White, S. H. *Proc. Natl. Acad. Sci. U.S.A.* **2005**, *102*, 15059–15064.

JP800162D

3. Simulations

Step 1: partitioning of ions into the sub-membrane space. This is simulated by a transient analysis, which performs an integration over time and thus yields the time course of the variables. The voltage source vbias is set to 0. The initial conditions $c_{K,in} = c_{Cl,in} = \Delta\varphi_m = \Delta\varphi_{sr} = 0$ need not be set because SPICE assumes zero voltages for all capacitors if not otherwise specified.

Step 2: repartitioning of ions due to different bias potentials. This is simulated by a transient analysis with the respective potential values assigned to the voltage source vbias. SPICE allows the setting of voltages across capacitors to be used as initial values for the transient analysis. Thus the initial conditions for $c_{K,in}$ and $c_{Cl,in}$ (0.1 M in the present case) are set as voltages at nodes K_in and Cl_in, respectively. Again the initial conditions $\Delta\varphi_m = \Delta\varphi_{sr} = 0$ need not be set.

Step 3: electrochemical impedance spectra. SPICE provides an ac small-signal analysis, which simulates EIS. However, this analysis cannot be used here because it is performed with the dc operating point of the circuit obtained in a respective analysis with "all capacitors opened".[1] Hence each frequency is simulated separately by a transient analysis. A sinusoidal AC voltage with amplitude 10 mV and the given frequency is added to the respective bias potential assigned to the voltage source vbias. Initial conditions are set as described above, in this case including $\Delta\varphi_m$ and $\Delta\varphi_{sr}$.

References

(1) Vladimirescu, A. *The SPICE Book*; Wiley: New York, 1994.

(2) Walz, D.; Caplan, S. R.; Scriven, D. R. L.; Mikulecky D. C. *Bioelectrochemistry: General Introduction*; Caplan, S. R., Miller, I. R., Milazzo, G., Eds.; Bioelectrochemistry: Principles and Practice Vol. 1, Birkhäuser: Basel, 1995; pp. 49.